THE ASTROPHYSICAL JOURNAL, 314:766–781, 1987 March 15

OBJECTIVE CHARACTERIZATION OF STELLAR ACTIVITY CYCLES. I. METHODS AND SOLAR CYCLE ANALYSES

RONALD L. GILLILAND
High Altitude Observatory, National Center for Atmospheric Research[1]
AND
SALLIE L. BALIUNAS
Harvard-Smithsonian Center for Astrophysics
Received 1986 March 21; accepted 1986 September 11

ABSTRACT

A large set of high-quality chromospheric activity index data of sufficient temporal extent to allow quantitative characterization of stellar cycles now exists thanks to the work, begun two decades ago, by Olin Wilson. In this paper we discuss the methods which can be used in analyzing the 18 yr records of Ca II H and K index data. The dominant noise source for most stars on cycle time scales is undersampled rotational modulation of stochastically distributed active regions. To set adequately statistical significances of power spectral peaks it is necessary to allow carefully for effects of the noise source. Sensitivity analyses with artificial records and tests with blocks of solar activity data show that the available 18 yr intervals are adequate for quantitatively characterizing solar cycle scale behavior in stars. A comparison of solar magnetic activity indices for the photosphere (sunspot areas), chromosphere (Ca II K-line emission) and corona (mean polarization brightness) is made and shows that quite similar cycle morphology exists for each measure.

Subject headings: Ca II emission — stars: chromospheres — stars: late-type — Sun: activity — Sun: chromosphere — Sun: corona — Sun: plages

I. INTRODUCTION

Wilson (1978) demonstrated in a seminal paper that several lower main-sequence stars showed spectrum variations in the Ca II H and K cores qualitatively similar to that shown by the Sun over the solar 11 yr cycle of chromospheric activity. As in the Sun, the stellar variations recorded by Wilson presumably serve as a proxy indicating the existence of magnetic activity cycles. Wilson (1978) obtained roughly monthly measures in 1 Å bands at the centers of the H and K lines for 95 lower main-sequence stars, over time intervals of 10–12 yr. This data set was sufficient for proving the existence of chromospheric activity variations on time scales of the solar cycle in stars other than the Sun.

The work of monitoring stars for indications of chromospheric activity has been continued at Mount Wilson by several collaborators. Much of the later work has concentrated on obtaining nightly observations in order to derive accurate rotation rates via rotational modulation of the chromospheric signal from stellar plages. Rotation periods have been measured for about half of the stars observed (Vaughan *et al.* 1981; Baliunas *et al.* 1983). Further work (Noyes *et al.* 1984) has shown that the mean chromospheric emission level is well correlated with the rotation period divided by the convective turnover time scale of the stellar envelope. This relation can predict the rotation rate from the stellar spectral type, absolute level of H and K emission, and models of the convective envelope characteristics.

Wilson's survey of lower main-sequence stars for long-term variations in chromospheric activity also has continued (Baliunas and Vaughan 1987; Baliunas *et al.* 1987). The large data set of chromospheric activity information has spurred attempts to understand the nature of stellar magnetic activity (Knobloch, Rosner, and Weiss 1981; Durney, Mihalas, and Robinson 1981; Noyes, Weiss, and Vaughan 1984).

With the availability of homogeneous data from 1966 to 1984 July, now is a propitious time to attempt a quantitative analysis of stellar cycles. The 18–19 yr data base with expected periods of 7–12 yr (Wilson 1978), is far more amenable to the study of stellar cycles than was Wilson's original temporal base of only 10–12 yr. The data and the first attempt to search for activity cycle periods are described by Baliunas *et al.* (1987). In this paper we present a more sophisticated technique to characterize stellar cycles, along with sensitivity analyses of artificial data and the analysis of several sets of activity measurements for the Sun. We shall show that derivation of accurate periods and characterization of cycle morphology (ratio of rise to decay time) is possible, but that the background noise, especially the growth and decay of activity, is an important and troublesome factor to consider. In a second paper we will apply this technique to the stellar data.

II. REALISTIC NOISE SIMULATIONS AND NUMERICAL EXPERIMENTS

a) What is a Stellar Cycle?

In order to characterize a stellar cycle we shall extrapolate from the solar case to define a working model of a stellar cycle. Skumanich *et al.* (1984) have developed a three-component model of the solar cycle variability of the 1.0 Å Ca II K emission (White

[1] The National Center for Atmospheric Research is sponsored by the National Science Foundation.

and Livingston 1978, 1981) using cell, network, and plage factors. At solar minimum the mean 1.0 Å K index can be well modeled by assuming a mix of a background component from cells (centers of supergranules) and network (supergranule boundaries). For the Sun as a star, the cell plus network components would not exhibit significant rotational modulation.

White and Livingston (1978, 1981) have shown that at disk center, outside of plage, the 1.0 Å K index does not vary from solar minimum to maximum. This suggests that the uniformly distributed (for the Sun as a star) cell plus network components are invariant over the period of observation. The increase of the 1.0 Å K index from solar minimum to maximum is 0.086–0.10 Å, or $\sim 16\%$ full amplitude modulation. Using extant contrast factors for plage, Skumanich *et al.* (1984) show that about half of the solar cycle variation can be directly accounted for by plage with the remaining half presumed to arise from enhanced network at high latitudes. The enhanced or active network is presumed to arise from the breakup of plage fields swept to supergranule boundaries. Therefore the totality of modulation over the solar cycle can be attributed directly, or indirectly, to the growth and decay of individual active regions. We therefore assume that a stellar cycle is formed periodically by the organized (i.e., nonrandom) appearance of active regions at the cycle period in time.

Given the above definition of a stellar cycle we must consider what happens when the distribution of active regions of finite lifetime is not ordered, as would define a true cycle, but purely stochastic. The latter defines the primary type of numerical experiment discussed below.

b) Periodogram Analysis

We adopt Scargle's (1982) formulation of power spectrum analysis as our basic data reduction tool. The time series of Ca II H and K line indices (S-index) at our disposal (Baliunas *et al.* 1987) is quite unevenly spaced. We form monthly averages for all data sets, but the coverage within a month is not uniform, and we retain use of the mean time of observations for each monthly average. The Scargle (1982) modification of the classical periodogram definition retains the simple statistical behavior of the evenly spaced case at only a slight increase in computational complexity.

Baliunas *et al.* (1985) and Gilliland and Fisher (1985) have described use of Scargle's (1982) periodogram technique in the analysis of S-index data for rotational modulation. For ease of reference and to define the notation we present the equations used. The periodogram as introduced by Scargle (1982) to deal with unevenly spaced data is (with modification for unequal weights)

$$P_x(\omega) = \frac{N}{2\sum_j W_j}\left\{\frac{[\sum_j X_j W_j \cos\,\omega(t_j-\tau)]^2}{\sum_j W_j \cos^2\,\omega(t_j-\tau)} + \frac{[\sum_j X_j W_j \sin\,\omega(t_j-\tau)]^2}{\sum_j W_j \sin^2\,\omega(t_j-\tau)}\right\}, \tag{1}$$

where τ is defined as

$$\tau = \frac{1}{2\omega}\tan^{-1}\left(\frac{\sum_j W_j \sin 2\omega t_j}{\sum_j W_j \cos 2\omega t_j}\right), \tag{2}$$

where $t_j, j = 1, 2, 3, \ldots, N$ are the observation times, X_j are the observed values, W_j are individual weights, N is the number of data points and $\omega = 2\pi f$ is an arbitrary test frequency. We use the weights, W_j, only as a simple means of removing outlying data points for which W_j is set to zero for points more than 3 σ from the mean. The weights could be used for application of window carpentry (see Scargle 1982) in order to control sidelobes of signal frequencies. Aliasing problems tend to be reduced by the essentially random distribution of t_j introduced by stellar observations scheduled (but never realized) on a nightly basis.

A signal-to-noise power ratio for the peak which is normalized to the background noise level is defined as (Scargle 1982)

$$p_0 = \frac{P_x}{P_N} = \frac{N}{4}\left(\frac{x_0}{\sigma_0}\right)^2, \tag{3}$$

where x_0 = signal amplitude and $P_N = \sigma_0^2$ is the variance of assumed Gaussian noise.

The root mean square frequency error of a given peak in the periodogram (see Kovacs 1981; Baliunas *et al.* 1985; Gilliland and Fisher 1985) may be approximated as

$$\frac{\Delta f}{f} = \left[\frac{0.0256}{(fT)^4} + \frac{0.5625\sigma_0^2}{N(fT)^2A^2}\right]^{1/2}, \tag{4}$$

where T = length of data set and A = signal amplitude. (We assume that the N measurements are independent. If autocorrelation exists in the noise source on the time scale of individual observations, the estimate of N should be correspondingly reduced.) Note that as fT, the number of cycles in the data set, decreases the frequency error rises linearly if noise dominated or rises quadratically if dominated by the first term which includes contributions from a possible background slope.

The distribution of peak heights in the periodogram (eq. [1]) is exponential for a time series of Gaussian noise. The *false alarm probability* that a peak as high or higher would occur by chance when the data are assumed to be Gaussian noise of the level indicated in equation (3) is (Scargle 1982)

$$Pr(p_0, N_f) = 1 - [1 - \exp(-p_0)]^{N_f}, \tag{5}$$

where $N_f \approx N/2$ is the effective number of frequencies sampled in the power spectrum (see Horne and Baliunas 1986). The primary problem encountered in determining Pr is deciding what to use for the noise variance for real data in which the partitioning of total variance between signal and random noise is not known *a priori*. Following the discussion in Scargle (1982) (see his eqs. [6]–[9]) we evaluate σ_0^2 as the *residual* variance after subtracting the primary frequency from the original data. The use of the total variance in estimating the false alarm probability has been discussed by Horne and Baliunas (1986). Our experience shows the difference in the

estimates of $P(\omega)$ between normalization by the total or residual variance is not a significant one compared to the effect of active region evolution as investigated in this paper. The dominant effect in producing spurious peaks in a test periodogram is long-lived active regions that randomly appear in relatively short spans of data. Numerical tests have demonstrated that the misleading periodogram peaks persist despite the different normalizations.

We tested the periodogram technique (eqs. [1] and [5]) by performing experiments with Gaussian noise. Figure 1 shows the distribution of the highest peak in the power spectrum of 50 realizations of time series dominated by Gaussian noise. The sampling was chosen from the actual distribution of observations for HD 155885 in the Mount Wilson *S*-index data set. As expected, the highest peak is uniformly distributed in frequency over the several realizations and has a distribution of false alarm probabilities corresponding to chance.

c) *Experiments with Realistic Noise*

The primary noise source we wish to investigate is that of randomly distributed active regions of finite lifetime over the time domain analyzed. If we correctly account for this type of noise, or, if the effect is negligible, an experiment (straightforward application of eqs. [1] and [5]) should produce results similar to those in Figure 1. To test our analysis system we wish to generate realistic experiments that closely match the stellar observational data. Since we wish to isolate potential problems which might be caused by active regions randomly distributed in time, we assume the test signals are unaffected by observational error. (Wilson [1978] and Baliunas *et al.* [1987] argued that many of the stars show signals dominated by intrinsic variations—far in excess of the 2%–3% observational error.)

We chose sampling dates that match the Mount Wilson time series of HD 155885 from 1966–1979. We selected a rotation period of 30 days for the star. We assumed an exponential active region lifetime, $\tau_{\rm growth}$, for each numerical experiment. The signal for each active region is decreased as exp $(-\tau_{\rm growth}/\Delta t)$ on both sides of a plateau of maximum light of length τ_P. We generated realizations of the light curve over 1966–1979 by summing the contributions of 150 active regions of finite pulses defined by $(\tau_{\rm growth}, \tau_P)$ that were stochastically distributed in time. Figure 2 shows three tests with $(\tau_{\rm growth}, \tau_P) = (25, 10)$, (50, 20), and (100, 40) days. The quantity τ_P represents time spent in a plateau of maximum light before the exponential dimming with a time scale $\tau_{\rm growth}$. Unlike the experiments with Gaussian noise these tests all show a distribution of highest peaks at low frequencies with false alarm probabilities much larger than expected from chance. *Thus, were we to naively apply periodogram analysis to these experimental time series (with* $\tau_{\rm growth} \geq 50$*) we would find signals of seemingly large significance at just the frequencies expected for stellar cycles!* We emphasize that *no* long-term activity cycle period was introduced into the simulated light curves. Inspection of Figure 2 shows that the anomalous signal is at periods greater than ~ 10 times the exponential growth-decay time scale. The derived anomalous power varies as the square root of active region lifetime. The effect is less sensitive to other parameters of the problem such as rotation period, number of active regions, or amplitude of individual active regions. We are faced with the need to alter the analysis in such a way that appropriate results for this type of experiment are obtained.

The effect of stochastically distributed pulses of finite lifetime can be understood heuristically in a simple way. The heart of the problem is the relatively short observing window, 18 yr, compared to the interference generated by the pulses. The signal generated is the sum of randomly distributed pulses convolved with the assumed profile of an active region in time. (The fact that the active regions occur on a rotating star is of secondary importance because of the short time scale of rotation.) The individual signals

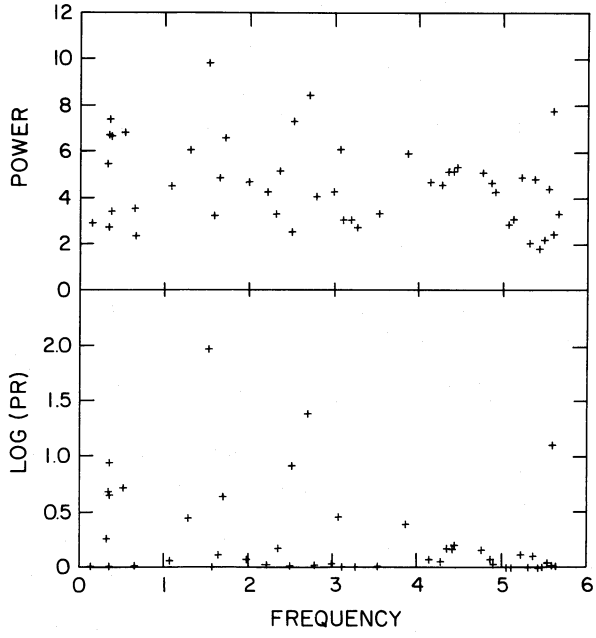

FIG. 1.—Distribution of the highest peak in power spectra of 50 Gaussian noise realizations. *Top*: power level, *Bottom*: $\log_{10}$ of the false-alarm probability (eq. [5]) vs. frequency in cycles per year.

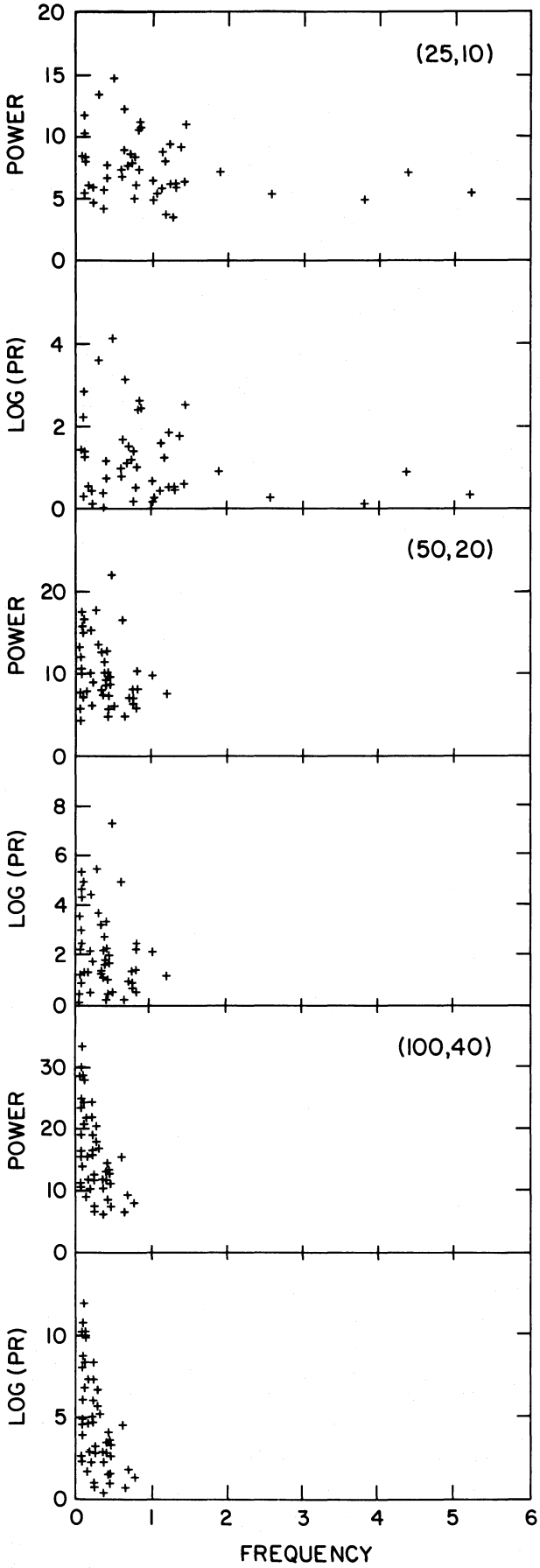

FIG. 2.—Distribution of the highest peak in 50 realizations of power spectra for stochastically distributed active regions with three different values of (τ_{growth}, τ_P) = (25, 10), (50, 20), and (100, 40) days from top to bottom. For each pair, upper panel shows power level, second panel shows $\log_{10}$ of false-alarm probability of both vs. frequency in cycles per year.

interfere *only constructively*, since the appearance of a plage can only give a positive, definite signal. A stochastic distribution of pulses will always have clumpiness. On time scales less than, or order of, the individual pulse profiles, no signal variations can be induced, no matter how clumpy the pulse distribution. The longer the lifetime of the pulses, the shorter the frequency at which structure can appear in the time series and the more pulse envelopes that will overlap. The overlap of the pulses that produces low-frequency peaks in the limited window of observations can be distinguished from true long-term periodicities with longer time series. Thus, both the shift to lower frequencies and increase of power levels with increasing active region lifetimes in the 18 yr data spans are easily conceptualized.

A stellar cycle is an organized clumping of active regions in the time domain. We must develop a discriminant to determine whether the signal for any given time series indicates a degree of clumping beyond that expected by mere chance from a random distribution. We seek a power-spectrum restoration process which will correctly allow the detection threshold and false alarm probability to be interpreted meaningfully. One technique is that of optimum restoration (Brault and White 1971), where the signal and noise can be separately identified in the Fourier domain, a filter designed, and a restored spectrum without the effects of noise extracted. Unfortunately, for any given realization of real signal plus "noise" from randomly distributed active regions, we have *no possibility* of disentangling the signal and noise, since both may have similar expected frequency distributions.

We can, however, correct for the threshold effect in an ensemble average sense. We define the mean power expected from randomly distributed active regions of an assumed lifetime by simply averaging together the power spectra from many realizations. If we assume the observed signal covariance is the convolution of the covariance of the true cycle signal with the covariance of the stochastically distributed pulses, then in an ensemble average sense we may correct for this by normalization of the power spectrum of the observed signal to the mean noise power spectrum. As a simulation this is illustrated in Figure 3. The upper panel shows the average power spectrum of 625 realizations of 25 randomly distributed active regions with $(\tau_{\text{growth}}, \tau_P) = (100, 20)$. (The "notch" at 1 cycle per year in the upper panel is the seasonal gap in the data and is discussed below.) The middle panels show the power and significance versus frequency of highest peak in each for 50 test cases with the same parameters as above. The lower panels show the resulting distributions for the highest peak after normalization by the mean spectrum (upper panel). We see that a roughly normal distribution is obtained.

We therefore adopt the following procedure to set the proper threshold accounting for the possibility of stochastically arrayed active regions.

Define

$$P_T(\omega) = \frac{1}{M} \sum_M P_S(\omega) , \tag{6}$$

where $P_S(\omega)$ = individual power spectrum (eq. [1]) of a time series realization, Z_i, of stochastically distributed active regions plus Gaussian noise. We set the time series of each realization as

$$Z_i = \sum_{N_A} a_0 \max [[0.0, \cos [2\pi(t_i - t_s)/P_{\text{rot}}] \exp \{-\max [0.0, \text{abs} (t_i - t_r) - 0.5\tau_P]/\tau_{\text{growth}}\}] + \sigma_0 R_i , \tag{7}$$

where N_A is the number of randomly distributed active regions, a_0 is the amplitude of rotationally modulated occluded cosine, P_{rot} is the stellar rotation period, t_i is the observation times of real data, τ_P is the assumed length of maximum intensity of active region, τ_{growth} is the exponential growth-decay time scale, t_s and t_r are randomly distributed values over domains P_{rot} and T (domain length), respectively, with different values for each active region, and $\sigma_0 R_i$ is Gaussian noise of standard deviation σ_0. Values of a_0 and σ_0 determine the relative contributions of rotationally modulated and Gaussian noise. We assume the observational noise is at 1% of S.

$$\sigma_0 = 0.01S \tag{8}$$

since the noise per observation is at 2%–3% (Wilson 1978) and a monthly average is typically composed of about five observations. The amplitude of assumed active regions is then chosen to account for the residual total variance (V) of the observed time series

$$a_0 = 2.56(V - \sigma_0^2)^{1/2} . \tag{9}$$

The observed power spectrum normalized to the threshold expected from stochastically distributed active regions is

$$P_R(\omega) = P_0(\omega)/P_T(\omega) , \tag{10}$$

where $P_0(\omega)$ is the periodogram of the observed time series. Note that this correction has the form of equation (3), with $P_T(\omega)$ a total noise component from the sum of stochastically distributed active regions plus Gaussian noise (eq. [7]). As demonstrated above, $P_R(\omega)$ yields a normal distribution of most significant peaks according to the false alarm probability criterion of equation (5).

The mean power spectrum, $P_T(\omega)$, of stochastically distributed active regions depends primarily on the assumed mean lifetime and also depends on the sampling distribution, stellar rotation rate, and averaging of data points in time before analysis. It is therefore necessary to generate the Z_i using the same sampling and averaging applied to the real data. The rotation period is either an observed quantity (Baliunas *et al.* 1983, 1987) or can be predicted from semi-empirical considerations (Noyes *et al.* 1984; Gilliland 1985). In general, we have no knowledge of the active region lifetime appropriate for a given star. We therefore evaluate different $P_R(\omega)$ for different assumed values of the lifetime. If the highest peak remains at the same frequency for different normalizations and maintains its high significance we can be confident (in a statistical sense) that the signal does not arise from a chance distribution of active regions. *If, however, the results are sensitive to the normalization used, we cannot have confidence that a real cycle exists.* Figure 4 illustrates values of $P_T(\omega)$ for additional lifetimes shorter and longer than those shown in Figure 3. As the

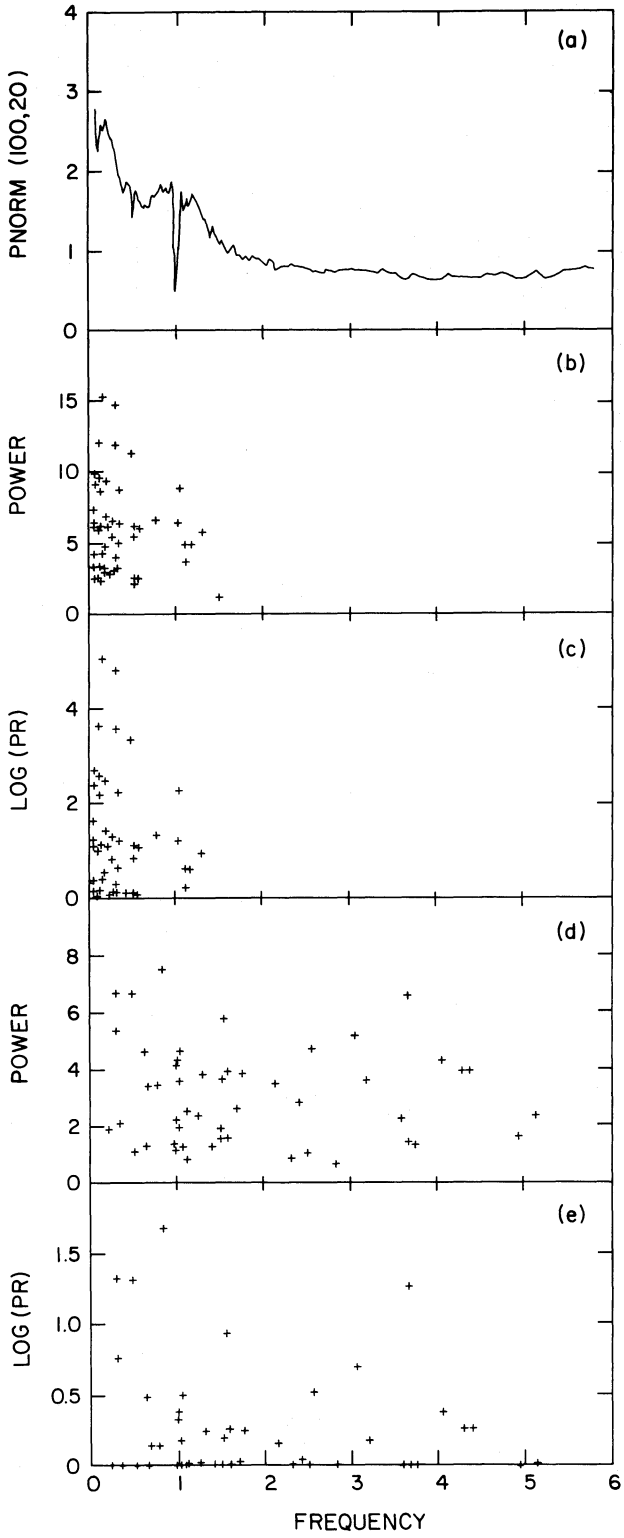

FIG. 3.—(*a*) Mean power spectrum (from eq. [6]) for randomly distributed active regions with (τ_{growth}, τ_P) lifetimes of (100, 20) days. (*b*)–(*c*) Power and false-alarm probability distributions for the highest peak in 50 realizations of power spectra from randomly distributed active regions with all properties the same as used to generate panel (*a*). (*d*)–(*e*) Distributions for highest power peak for the same 50 realizations after first normalizing by the mean spectrum of panel (*a*) (see eq. [10]).

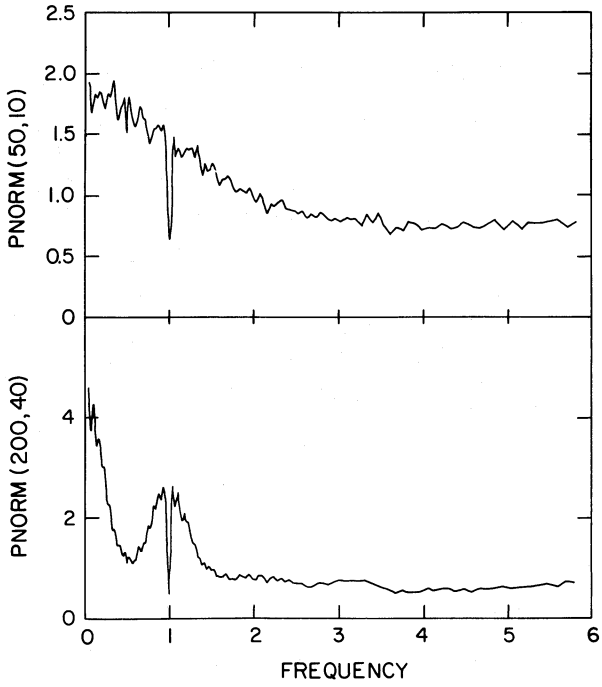

FIG. 4.—Two additional normalization mean spectra (eq. [6]) are shown at (τ_{growth}, τ_P) lifetimes of (50, 10) and (200, 40) days in top and bottom panels, respectively. All other conditions match those used in Fig. 3.

lifetime of the active regions drops to about one month, the mean spectrum approaches that of Gaussian noise—equal to 1.0 at all frequencies. The lack of power at one cycle per year results from the seasonal nature of the observations which are generally obtained for the same few months each year. The "shoulders" near one cycle per year in the lower panel of Figure 4 result from aliasing of low frequencies with the observing window. From Figures 3–4 it is obvious that peaks in a direct power spectrum near one cycle per year or less than ~ 0.3 cycles per year are suspect. This leaves perios of ~ 1.5–3.5 yr as most reliably detectable given the existing data set. Year-round sampling would remove complications near one cycle per year. The problem at low frequencies improves in two ways with longer data sets: (1) the mean power at a given frequency due to stochastically distributed pulses drops and (2) with more data the power level resulting from a real signal will grow with respect to the background. In later sections we will analyze how serious the above problems may be for the Mount Wilson data sets which are only 18–19 yr long.

III. AUXILIARY ANALYSES

In order to discuss the amplitude and morphology of possible stellar cycles we will fit cosine and sawtooth functions to the observed S-index data. We have tested this method with synthetic time series. The frequency of maximum power from the periodogram is used as an initial guess for the nonlinear least-squares solution. Both the cosine and sawtooth fits are evaluated with simultaneous solution for zero point offset and a linear background trend (first two terms below). The sawtooth function is represented as

$$y(t_i) = b_0 + b_1(t_i - t_0) + s(P, A, X, t_0; t_i) ,$$

where

$$\begin{aligned} s(t_i) &= \frac{AZ}{X} && Z \le X \\ &= A\left(1. - \frac{Z - X}{1. - X}\right) && Z > X \end{aligned} \tag{11}$$

with

$$Z = \frac{t_i - t_0}{P} - \mathrm{INT}\left(\frac{t_i - t_0}{P}\right)$$

with A = amplitude, P = period, t_0 = phase at beginning of rising branch, and X = fraction of cycle spent on the rising branch. In practice t_0 must be chosen such that $t_i - t_0$ is always positive. The sawtooth function objectively characterizes the rate of growth to decline for the cycle. Visual inspection of the S-index time series for many stars (Wilson 1978) suggests that a sawtooth function is appropriate to describe cycle shape and that large variations from one star to another in the rate of rise and decline in fact exist.

Probable errors of a given parameter are estimated as the increment that would result in an increase of χ^2 by unity (Bevington 1969). In practice this procedure works well in cases with high signal-to-noise (S/N) ratios with obvious signals. At lower S/N ratios the error evaluation loses stability. Conservatively applied subjective judgment, based upon experience analyzing a large number of synthetic time series, must ultimately be used to consider the reliability of individual estimates.

IV. SENSITIVITY TESTS

As was demonstrated in § II the analysis and estimation of significance levels for stellar cycle periods cannot be reliably executed with naively applied standard techniques. To gain insight into the interpretation of results one is forced to generate synthetic time series in which the signal and noise characteristics are at the investigators control, and these may be used to optimize and calibrate the reliability of reduction techniques.

We have thoroughly investigated the detectability and characterization of stellar cycles over a wide range of parameter changes including S/N ratio, length of period with respect to length of observing domain, phase of input signal, and shape of input sawtooth function. All synthetic time series used the actual observing dates for a star (usually HD 155885 or HD 201091) in the Mount Wilson data set. Noise is included both from rotational modulation of stochastically distributed active regions and Gaussian noise (see eq. [7]). Normalizations for active region lifetimes as in equation (10) were applied to all simulation test power spectra, just as will be done for analysis of real data. We examined three power spectra for each case: (1) no normalization—equivalent to the assumption of Gaussian noise, (2) normalization assuming $(\tau_{\rm growth}, \tau_P) = (50, 10)$ for stochastically distributed active regions, and (3) normalization assuming $(\tau_{\rm growth}, \tau_P) = (250, 50)$. This range of assumed lifetimes generates the full range of $P_T(\omega)$ morphology from equation (6) and brackets the exponential decay time of plage observed area of 43 days (Allen 1973) for the Sun. We will not attempt to detail the results of our final sensitivity tests, which numbered over 30, each with 50 realizations but will summarize the conclusions.

For the S/N ratio tests we have assumed rotational and Gaussian noise components in the ratio of 4 to 1. We define the noise simply as the standard deviation of total noise and signal as amplitude of cosine input signal or half the amplitude of a sawtooth cycle. With an input cycle period of 11.5 yr, random phases of cycle periods and an 18 yr observational domain the correct signal is found for 67% of cases with the $\tau_{\rm growth}, \tau_P = (50, 10)$ normalization and S/N ≈ 1; the normalization at (250, 50) results in essentially zero percent success rate. At S/N ≈ 2 the success rate is 100% with the (50, 10) normalization but still poor at the (250, 50) normalization. For successful detection under the assumption of $\tau_{\rm growth}, \tau_P = (250, 50)$ a S/N $\gtrsim 4$ is required. For the S/N ≈ 2 case the derived periods are in error by 0.04 ± 0.66 yr, while equation (4) indicated an expected error of 0.9 yr (this allows for possibility of nonzero background slope which was not included in generating the test series). At an input signal of 4.0 yr, 96% success is attained at S/N ≈ 2 and (50, 10) normalization—mean errors are 0.00 ± 0.06 with an expected error of 0.05. With a S/N ≈ 2 periods at 1.8 and 0.7 yr are detectable at $\sim$98% success rate for the (50, 10) normalization with error as expected from equation (4). In general a S/N $\gtrsim 2$ is sufficient for detection of cycles with $P < 12$ yr. A value of S/N ≈ 1 can reliably yield success for periods in the 1.5–4.0 yr range because the mean normalization power spectra approach unity. Figure 5 shows the results of 50 realizations with P randomly distributed between 0.5–17.5 yr for a S/N ≈ 2. Two points are obvious from Figure 5: (1) the errors increase rapidly for longer periods and (2) normalization by $P_T(\omega)$ generated with long active region lifetimes results in a high failure rate for $P \gtrsim 5$ yr.

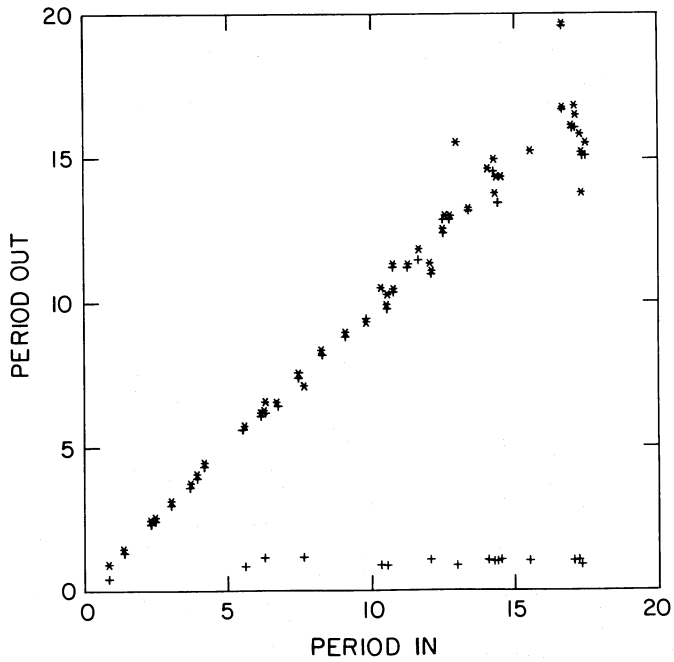

FIG. 5.—Results of sensitivity test with S/N = 2.0 and randomly distributed input cycle periods (in years) plotted vs. the derived period. Asterisks and plus signs respectively, represent normalization by $(\tau_{\rm growth}, \tau_P) = (50, 10)$ and (250, 50).

Where normalization results in a highest peak not corresponding to the input period, the erroneous period often falls near 1 yr—a further indication that the seasonal sampling destroys the possibility of detecting real variations near ~ 1 yr.

Tests with input periods of 11.5 and 4 yr were conducted with random cycle phases relative to first observation time. There were no large-scale systematic errors as a function of input phase.

To determine how well the sawtooth shape parameter could be recovered we generated such signals with X (eq. [11]) randomly chosen between 0.1 to 0.9. At a S/N ≈ 1.5 and $P = 10$ yr, the mean error on derived X was 0.15. The periodogram analysis picked out the correct cycle period for normalization at (50, 10) (error on $P = 0.02 \pm 1.5$ with expected error of 0.7 yr) in all cases, with a moderate failure rate at (250, 50). For this low S/N test case the errors on X are such that (1) for X input ~ 0.4–0.6 its measured scatter is random at about ± 0.05; (2) as X approaches 0.1 or 0.9 the errors increase up to ~ 0.4 and are skewed to $X_{\rm out} \approx 0.5$. Errors on X are thus conservative in the sense that real deviations away from $X = 0.5$ are underestimated. At a S/N = 3.0 the same test yields a mean error on X of ± 0.05 which is now not skewed toward 0.5 or larger in amplitude as $X = 0.1$ or 0.9 is approached. In this case the period errors were -0.2 ± 0.44 with an expected standard deviation of 0.6. Therefore a S/N greater than 2 is required for any confidence in the derived sawtooth-shaped parameter. Use of sawtooth input cycles does not result in a serious degradation of the periodogram success rate versus cosine inputs.

It is worth noting that a S/N = 1 will typically result in a periodogram peak level of $N/4$ (eq. [3]); for typical stars from the Mount Wilson data set this will result in a peak power of ~ 25, which would be quite significant by equation (5). At low frequencies the normalization of equation (10) will result in a factor of 1.5–4 decrease, thus resulting in a moderate to low significance estimate. The estimated power grows quadratically with improving S/N—resulting in reliable detection for S/N $\gtrsim 2$. For cases in which no real signal exists the derived S/N for the most prominent frequency will rarely exceed unity.

We have shown that detected signals with S/N significantly in excess of unity are likely to be real and that our methods of estimating cycle properties produce parameter estimates with known error properties. We are now in a position to analyze real data on solar cycle modulation for future comparison with stellar data.

V. TESTS ON A LONG RECORD OF SOLAR ACTIVITY

We now analyze a series of short blocks of data extracted from a much longer sequence of solar activity data for four purposes: (1) to determine how well the solar cycle can be detected with limited data lengths, (2) to test the data's sensitivity to variations in the sampling times and block lengths, (3) to quantify parameters of the solar cycle for comparison with stellar cycles, and (4) to quantify the variance in cycle properties with time for the only case in which this is currently possible—the Sun. We have adopted the longest instrumental record of solar activity available—the reconstructed solar constant over 1874–1982 by Hoyt and Eddy (1982). Details of the argument claiming the sunspot blocking can be used to predict solar constant variations accurately remain controversial. The index *is*, however, a direct measure of projected sunspot areas, with limb darkening and contrast factors included, which should provide an excellent, homogeneous record of how a sunspot index would have varied for the Sun observed as a star. The monthly averaged record, shown in Figure 6, covers ~ 10 solar cycles.

The solar series that most closely matches the stellar time series is 18 yr blocks of five consecutive monthly average data points per year. We used 46 consecutive samples taking 2 yr steps through the full data set. This sampling is highly overlapped and will be used to illustrate variations in cycle parameters and the insensitivity to phase of cycle with respect to the start of time series. The distribution of sample dates is kept the same for each of the 46 blocks; therefore the mean normalization spectra (to correct for detection threshold due to possibility of stochastically distributed active regions) will be the same for each block. Figure 7 illustrates the results for this analysis series. The normalization power spectra were generated with values of $(\tau_{\rm growth}, \tau_P) = (30, 10)$ and (90, 30). The first of these approximates the solar active region lifetime, while the latter is used to demonstrate effects of assuming a longer lifetime. The detected periods are shown for the unmodified and two normalized power spectra. The only failures to detect correctly

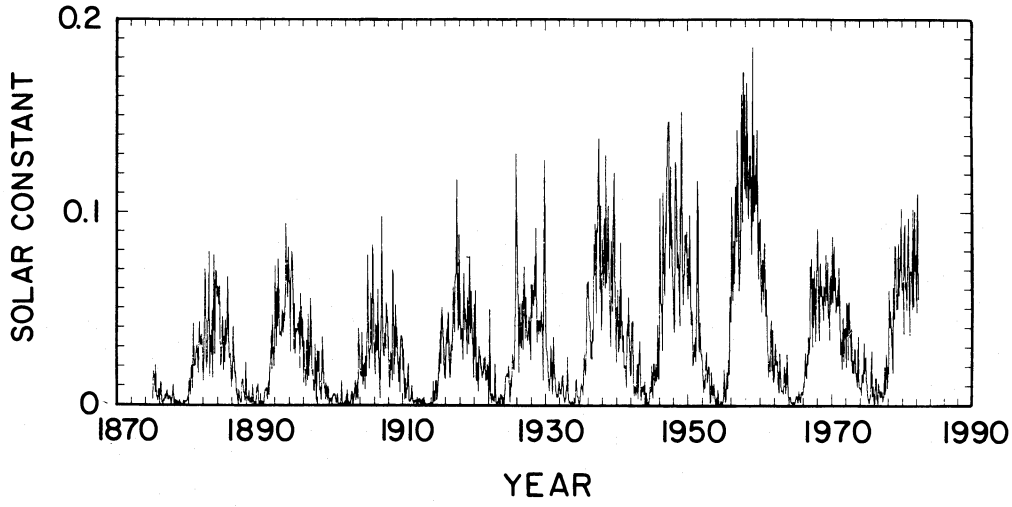

FIG. 6.—Monthly average values of reconstructed solar constant (in percentages of negative deviations) from Hoyt and Eddy (1982). This is used as a long-term, homogeneous record of sunspot activity as would be seen for the Sun as a star.

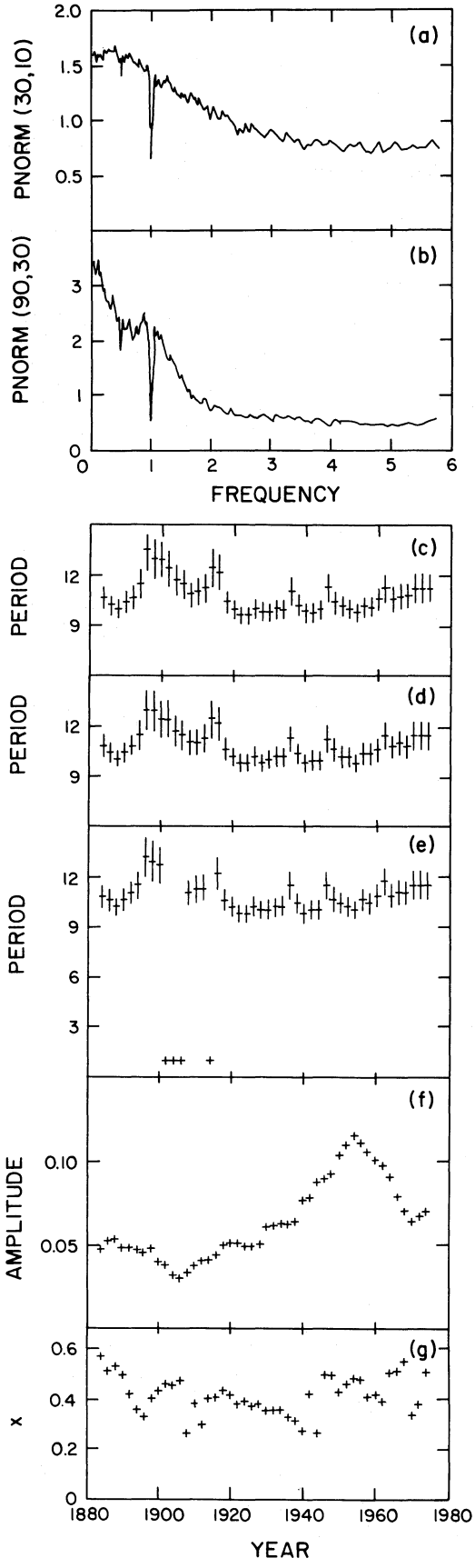

FIG. 7.—Analysis of 18 yr blocks of monthly average solar constant with five months per year. (*a*)–(*b*) show normalization spectra of (τ_{growth}, τ_P) lifetimes of (30, 10) and (90, 30), respectively. (*c*) Period of maximum power for unmodified periodogram. (*d*)–(*e*) Distribution of derived periods after normalization by mean spectra of panels (*a*) and (*b*), respectively. (*f*) Full amplitude modulation for a nonlinear least-squares cosine fit. (*g*) Sawtooth function parameter X.

the solar cycle occur for four cases in the early 20th century (a time of weakest signal—see Fig. 6) with the long active region lifetime normalization. Alternative normalizations do not significantly alter the derived periods. The error bars in Figure 6 are $\pm 1\ \sigma$ (eq. [4]) and demonstrate that significantly different values for the solar cycle period have occurred over the last century. The minumum detected period is $\sim 9.8 \pm 0.5$ yr, with a maximum period of $\sim 13.0 \pm 1.0$ yr. The mean is 10.88 ± 0.86 yr, while the mean error estimate is 0.75 yr from equation (4) and 0.54 yr for the least-squares sawtooth fit. The instantaneous amplitude varies over a factor of ~ 4. Only seven out of 46 samples have $X > 0.5$; the mean $X = 0.42 \pm 0.08$ demonstrates the known tendency of the solar cycle to rise rapidly and slowly decline (Waldmeier 1955). The average S/N is 2.1 with mean power level of 65 after the (30, 10) normalization.

If 12 yr blocks of five months each are used, the failure rates for detection of the solar cycle are $\sim 10\%$ and $\sim 50\%$ for the (30, 10) and (90, 30) normalizations, respectively. Errors on derived periods double with respect to the 18 yr block solutions, and solutions for the amplitude show a large scatter, instead of smooth trends. While the correct cycle length is usually detected with only a 12 yr domain, characterization of its parameters is not stable.

The use of all 12 months for 18 yr blocks does not yield significantly different results from five months per year over 18 yr. Figure 8 shows the normalizations for this sampling—the bias near 1 cycle per year has disappeared. Although the second normalization is higher at low frequency than for the five-month sampling, the power of a real signal is correspondingly increased. With this sampling, 100% success in detection is attained for each normalization—that is a slight improvement. Parameter estimates are not significantly altered, although the error estimates drop by 10%–50% versus the five-month solution. The derived X is 0.39 ± 0.08 with only three of 46 points above 0.5 and extreme values of 0.23 to 0.51.

Figure 9 illustrates the results obtained if an interval of five-months per year over 36 yr is used. The primary difference with respect to results over 18 yr blocks is much improved error estimates. (Only 36 samples with much increased overlap exist for this case.) The mean cycle period is 10.74 ± 0.62 yr with expected mean errors of 0.19 (eq. [6]) and 0.12 from least-squares fit of a sawtooth function and a full range of 10.0–12.0 yr. The quantity X is 0.35 ± 0.06 with no values above 0.5 and a range of 0.28–0.50.

As an example of the details that cannot be detected in currently available stellar data, we have analyzed the full solar data set taking six-month averages. The power of the normalization spectra decreases to a uniform value of ~ 2 over the frequency range of interest for the $(\tau_{\rm growth}, \tau_P) = (90, 30)$ active region lifetime assumption. Figure 10 shows the power spectra of the original data set, its cosine fit, and repeated analysis on the residuals after subtracting the best cosine fit. In addition to the primary period at 10.7 ± 0.06 yr, there is a statistically significant, second maximum at 9.62 ± 0.06 yr; no further peaks are significant. The two frequencies were in phase in the 1950's and have a beat period of ~ 93 yr—this may help explain the variation of amplitudes seen in Figures 7 and 9. (The converse is not true: if the data are first normalized by the instantaneous amplitude of Fig. 7, the 10.74 and 9.62 yr periods are still detected. Therefore the 9.62 yr period is not the result of amplitude modulation of the primary frequency.)

An analysis of residuals for the five-month, 18 yr sampling results in no detections of significant secondary peaks. The false alarm probabilities for the 46 samples are distributed as expected from chance. We would not expect detection of individual 10.74 and 9.62 yr signals of different amplitude in only 18 yr blocks. Further discussion of the significance of multiple periodicities in the Sun is beyond the scope of this paper, but no evidence on such subtleties can be expected from stellar analyses in the near future because long time series have not yet been obtained.

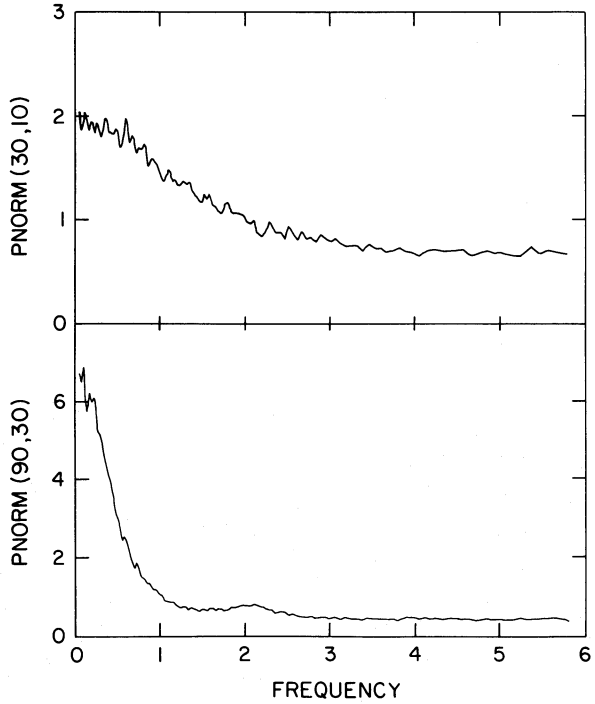

FIG. 8.—Same as Figs. 7*a*–7*b*, but for sampling at 12 months each year over an 18 yr domain

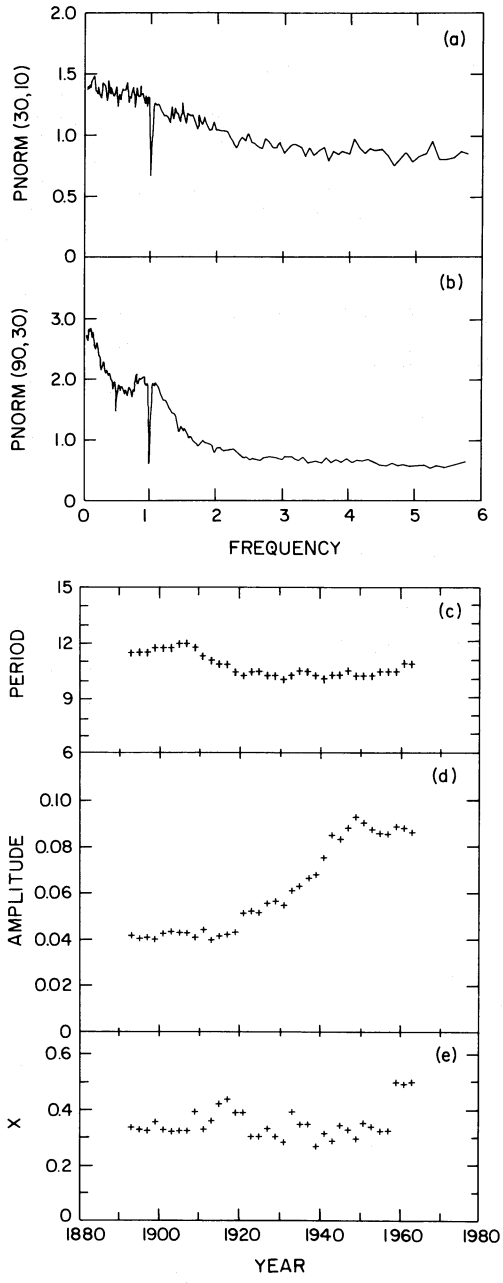

FIG. 9

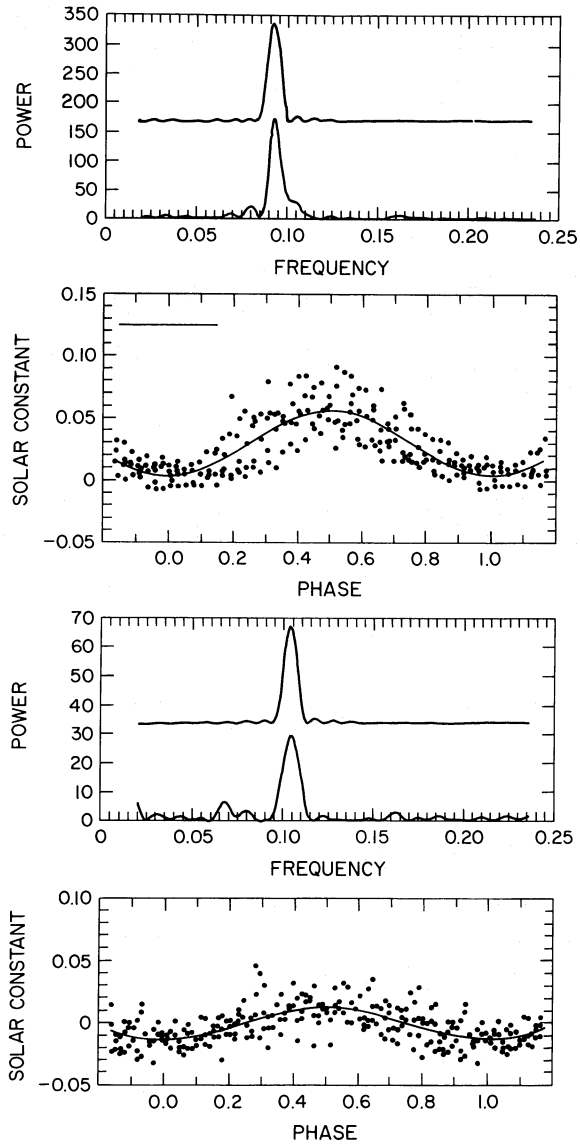

FIG. 10

FIG. 9.—Analysis of 36 yr blocks of monthly average solar constant with 5 months per year. (*a*)–(*b*) show normalization spectra at (τ_{growth}, τ_P) lifetimes of (30, 10) and (90, 30), respectively. (*c*) Period of maximum power for case normalized by mean spectrum of (*a*). (*d*) Full amplitude modulation for a cosine function fit. (*e*) Sawtooth function parameter X.

FIG. 10.—*Upper panels*: analysis of solar constant data over 1875–1982 in six-month averages. Upper spectrum is of least-squares cosine fit (plotted as curve in second panel). Note excess power in high-frequency wing of main feature of lower power spectrum of real data. *Second panel*: superposed epoch plot at derived period of 10.7 yr; nearly horizontal line at upper left shows background slope removed during fit. *Lower panels*: same analysis after subtraction of $P = 10.7$ yr cosine fit. The residual 9.62 yr period is statistically significant.

VI. COMPARISON OF SOLAR RESULTS FOR INDEPENDENT, RECENT EPOCH INDICES

a) The Photosphere—Sunspot Area Index

We have chosen to analyze the period of 1965 June through 1984 November. This domain matches the availability of data for the corona (discussed below), is roughly the length of the Mount Wilson stellar S-index time series, and marginally covers two complete solar cycles. We use monthly average values of reconstructed solar constant from Hoyt and Eddy (1982) with extensions through 1984 from Eddy, Hoyt, and Gilliland (1987). As discussed in § V, this is a good sunspot index for the Sun as a star, whether or not it represents solar constant variations via the sunspot blocking mechanism.

Figure 11 shows the basic plot which will be produced during the reduction of all solar and stellar cycles related data. Monthly and yearly data means are shown along with the power spectrum [normalized to assumed active region lifetimes of $(\tau_{\rm growth}, \tau_P) = (30, 10)$ as in eq. [10]), a power spectrum of best least-squares model, and least-squares regressions with cosine and sawtooth (eq. [11]) functions. The solar cycle period derived from the sunspot area index is 11.3 ± 0.4 yr with a S/N ≈ 2.4. Epoch of minimum is estimated as 1975.3 from the cosine fit and 1976.6 from the sawtooth function analysis. The tendency for a rapid rise and slow decline is quantified as $X = 0.28 \pm 0.04$.

If the reconstructed solar constant (see Eddy, Gilliland, and Hoyt 1982 for a general discussion) represents real luminosity variations with an $\sim$25% or smaller error, then measurement of broad-band intensity to a precision of $\sim$0.02% or less per year would be sufficient to determine and quantify the presence of stellar cycles for solar-like cases. Since the Sun may fall at the lower range of amplitude of typical cyclic behavior, such precision should be adequate for detecting stellar cycles. One of us (R. L. G.) is collaborating with John McGraw to use CCD transit photometry data (see McGraw *et al.* 1982) to search for stellar cycles in a large ($>10^3$) number of late-type stars. The simultaneous observation of a large number of stars should enable corrections for short time-scale sky transparency variations to be made through the assumption of a constant ensemble average, thus enabling photon statistics limits of $\sim$0.2% per night to be reached. With a dedicated instrument order of 100 observations on a given star may be obtained per season, thus allowing the 0.02% per year precision domain to be reached.

b) The Chromosphere–1 Å Ca II K Index

The solar chromospheric index of White and Livingston (1978, 1981) is directly analogous to the Mount Wilson *S*-index for stars. Unfortunately, uniform, dense coverage was only begun in 1976. We make use of the data from 1976 January to 1984 November provided by Oran R. White. The $\sim$9 yr length is marginal for attempts to characterize solar cycle behavior.

Figure 12 shows the 1 Å Ca II K index (equivalent width of central 1 Å emission), power spectrum, and least-squares analyses. The periods are smaller than for the analysis of 20 yr worth of data on the solar constant but not significantly so given the larger errors. The derived sawtooth shape parameter, $X = 0.52 \pm 0.16$, has too large an error to tell us anything significant about the solar cycle. The S/N is $\sim$2.7—comparable to the value for solar constant variations. Analysis of the reconstructed solar constant over the same

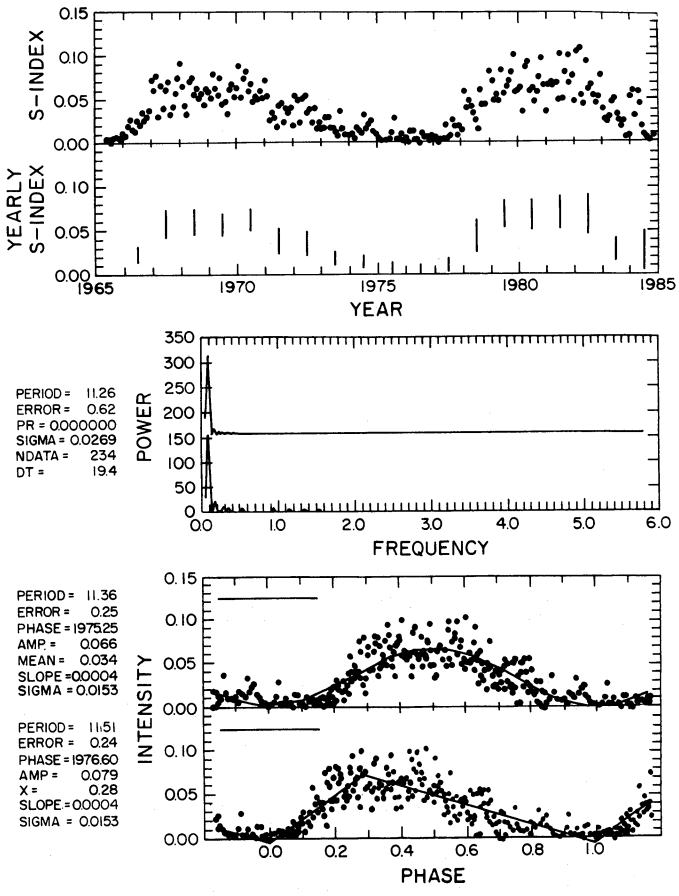

FIG. 11

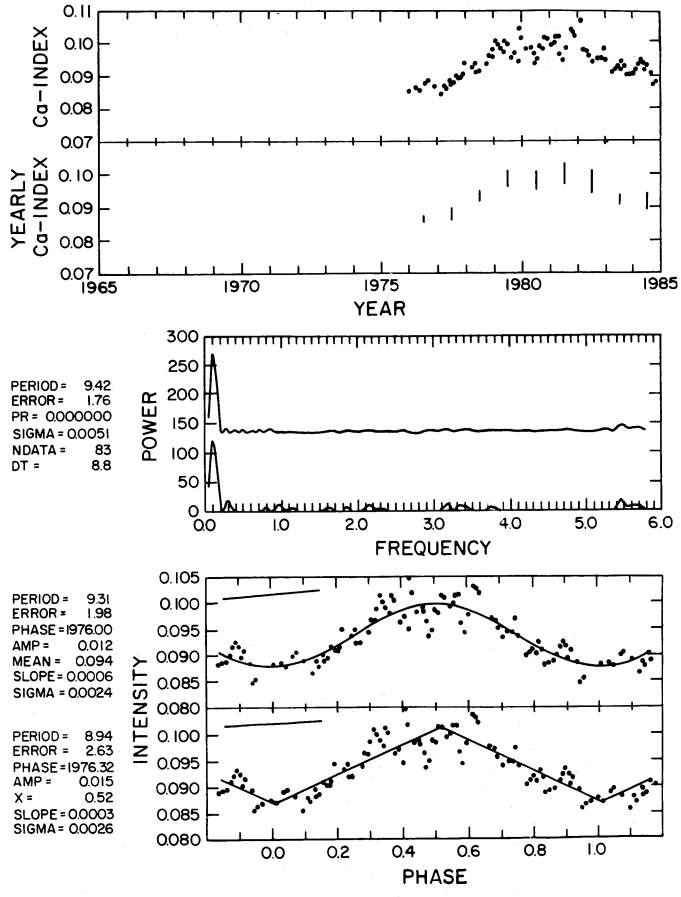

FIG. 12

FIG. 11.—Analysis of recent epoch reconstructed solar constant data. *Upper panel*: monthly means and yearly averages (plotted as $\pm 1\ \sigma$ from mean). *Middle panel*: power spectrum of data (*bottom*) and least-squares fit (*top*). *Lower panel*: superposed epoch plots of cosine (*top*) and sawtooth function (*bottom*) fits. Lines at upper left illustrate slope removed before generating plot. Information listed to the left of lower panels refers to adjacent plot and should be self-explanatory.

FIG. 12.—Same as Fig. 11 but for solar Ca II 1 Å K index from O. R. White and W. C. Livingston

1976–1984 time domain produces very similar results, suggesting that the gross physical characteristics of the solar cycle as evidenced by photospheric and chromospheric indices is virtually identical.

c) *The Corona–pB Index*

The corona exhibits variations over the solar cycle (Fisher and Sime 1984). We analyzed a record of mean, monthly polarization-brightness (pB) measurements derived from a series of K coronameters over the period 1965 June–1984 November. (The value of pB is proportional to mean hemispheric coronal electron density.) The recent epoch data was provided to us by Richard Fisher and David Sime. The data (pB in units of 10^{-8} disk $B_{\odot}$) are shown in Figure 13. The gaps occurred during the installation of new instruments. Calibrations of the three independent time series to a common standard have been made (Fisher and Sime 1984), but systematic errors at the 10% level between blocks could easily exist.

The periods derived from the coronal data exceed those from the solar constant analysis but only at the 1–2 σ level. Analysis of the solar constant data only during the dates when pB measurements were available produced results nearly identical to the ungapped solar constant data. This suggests that the gaps do not adversely effect the analysis. Phases of cycle minimum do not differ significantly from the photospheric results. The cycle shape does, however, show a significant difference with $X = 0.17 \pm 0.03$, suggesting that the mean coronal electron density at a height of $\sim 1.5\ R_{\odot}$ shows a more rapid rise from solar minimum to maximum than does the sunspot area. The S/N of the coronal pB cycle is ~ 2.0, only slightly smaller than the photospheric and chromospheric values. The lower S/N could easily result from the gaps at solar maximum and possible calibration errors.

d) *Discussion*

In Figure 14 we show the reconstructed solar constant, Ca II K index, and coronal pB co-plotted after linear transformation of each set such that the minimum value equals zero and amplitudes are similar. Figure 14 illustrates the main points quantified above. *The most basic point is that the photospheric, chromospheric, and coronal manifestations of magnetic activity associated with the solar cycle show quite similar behavior.* The only noticeable difference is the tendency for coronal densities to rise more rapidly than sunspot areas—suggesting a difference in growth rates for the large scale structures influencing the corona with respect to the smaller scale photospheric features.

Another feature obvious from Figure 14 (also see Figs. 11–13) is that the intermonth variability is strongly modulated (>factor of 2) over the solar cycle and the scatter at maximum is comparable to the cycle amplitude. This may be quantified by cross-correlating the amplitude versus scatter in 10 phase bins over the cycle. As an average over cosine and sawtooth fits the linear correlation

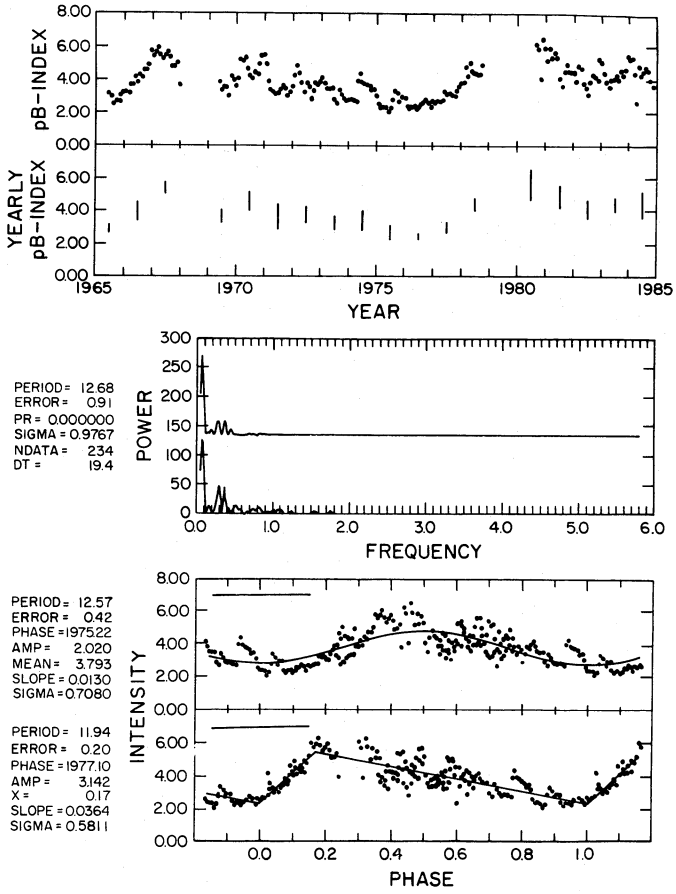

FIG. 13.—Same as Fig. 11 but for solar pB index from R. Fisher and D. G. Sime

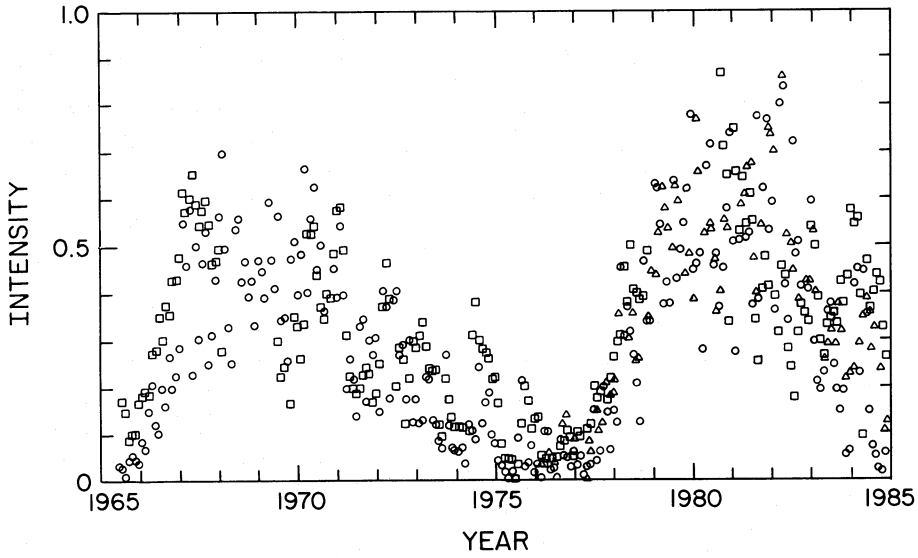

FIG. 14.—Simultaneous plot of monthly average solar constant (*circles*), Ca II K (*triangles*), and pB (*squares*) data after subtracting minimum value from each set and scaling to bring mean level of indices into registration.

coefficient and phase lags are (0.84, 0.09), (0.68, 0.05), and (0.69, 0.02) for the photospheric, chromospheric, and coronal indices, respectively. All of the correlations are significant at the 95% level with the scatter tending to peak later in the cycle by phase 0.02–0.09 or 0.2–1.0 yr. *The modulation properties of each index are remarkably similar both in terms of cycle S/N and the morphology of scatter variations with respect to cycle phase.* The positive correlation of scatter versus amplitude at essentially zero lag supports the contention that *the solar cycle is an organized periodic clumping of individual activity pulses as opposed to a smooth variation of a global property over the cycle.* The relationship of scatter and amplitude for stellar cycles should be investigated as another property comparing solar and stellar magnetic activity.

Throughout our analyses we have applied statistical tests based upon a uniform (stochastic) distribution of activity pulses in time, developing corrections to standard analyses such that significant cycles will not be claimed when such do not in fact exist. We have not directly tested the conclusion that the solar cycle is an organized periodic clumping of activity pulses via simulations with periodically clumped pulses. The solar analyses demonstrate, however, that cycles presumably composed of periodic clumping of activity pulses are readily detectable and quantifiable. To fully quantify cycle amplitudes and noise properties would require the analysis of further data simulations in which a signal composed of periodically clumped activity pulses is used.

The increase of intermonthly scatter carries information on both the lifetime of activity pulses and the mean number of pulses simultaneously present. A large increase of monthly scatter, as seen for the Sun, implies (1) a lifetime of active regions less than or of order one month for modulation to exist on this short of a time scale and (2) a signal that is dominated by only a few activity centers at maximum, since a large number would produce only $1/N^{1/2}$ modulation, whereas order unity modulation is actually present.

VII. CONCLUSIONS

We have quantified the extent to which stellar cycle properties can be derived from data sets of various S/N properties of different lengths. In particular, we have demonstrated that 18 yr blocks of data (the length of stellar Mount Wilson *S*-index) reasonably characterize the solar cycle, whereas 12 yr blocks (as available to Wilson 1978) were of much poorer quality in terms of quantifying aspects of the solar cycle. With data sets covering 18–19 yr for some 100 stars this is a propitious time to perform a quantitative analysis of stellar-cycle properties.

Under the assumption that a stellar cycle is composed of a temporal clumping of discrete events, we showed that this property determining the noise characteristics must be dealt with in order to derive realistic estimates of statistical significance for the existence of individual cycles. This correction to the threshold level of cycle detection significance can be attained by normalizing the power spectrum of an observed time series to the mean power spectrum of simulated time series composed of stochastically distributed active regions of assumed lifetime. If the significance of a power spectrum peak is sensitive to the choice of different, but reasonable, assumed active region lifetimes, then we cannot have confidence in detection of a real stellar cycle.

We quantified the degree of variability of the solar cycle over a 107 yr interval using a sunspot-area index. For the recent epoch photospheric, chromospheric, and coronal activity indicators show quite similar behavior.

We thank O. R. White and W. C. Livingston for providing the solar Ca II K data set prior to publication. We thank R. Fisher and D. G. Sime for providing the data set of coronal densities through 1984 November. J. A. Eddy and D. V. Hoyt made possible the extension of reconstructed solar constant through 1984. We thank T. M. Brown, J. A. Eddy, R. Fisher, D. Mihalas, D. G. Sime, and O. R. White for useful discussions and R. Fisher and an anonymous referee for comments on the manuscript. We gratefully acknowledge support from the National Science Foundation (AST 81-21726), National Geographic Society (2548-82), the Scholarly Studies Program and Langley-Abbot Fund of the Smithsonian Institution, and the Carnegie Institution of Washington.

REFERENCES

Allen, C. W. 1973, *Astrophysical Quantities* (London: Athlone Press).
Baliunas, S. L., *et al.* 1983, *Ap. J.*, **275**, 752.
———. 1985, *Ap. J.*, **294**, 310.
———. 1987, in preparation.
Baliunas, S. L., and Vaughan, A. H. 1987, in preparation.
Bevington, P. R. 1969, *Data Reduction and Error Analysis for the Physical Sciences* (New York: McGraw-Hill).
Brault, J. W., and White, O. R. 1971, *Astr. Ap.*, **13**, 169.
Durney, B. R., Mihalas, D., and Robinson, R. D. 1981, *Pub. A.S.P.*, **93**, 537.
Eddy, J. A., Gilliland, R. L., and Hoyt, D. V. 1982, *Nature*, **300**, 689.
Eddy, J. A., Hoyt, D. V., and Gilliland, R. L. 1987, in preparation.
Fisher, R., and Sime, D. G. 1984, *Ap. J.*, **285**, 354.
Gilliland, R. L. 1985, *Ap. J.*, **299**, 286.
Gilliland, R. L., and Fisher, R. 1985, *Pub. A.S.P.*, **97**, 285.
Horne, J. H., and Baliunas, S. L. 1986, *Ap. J.*, **302**, 757.
Hoyt, D. V., and Eddy, J. A. 1982, *NCAR Tech. Note*, TN-194+STR.
Knobloch, E., Rosner, R., and Weiss, N. O. 1981, *M.N.R.A.S.*, **197**, 45P.
Kovacs, G. 1981, *Ap. Space Sci.*, **78**, 175.
McGraw, J. T., Stockman, H. S., Angel, J. R. P., Epps, H., and Williams, J. T. 1982, in *Proc. Soc. Photo-Opt. Instrum. Eng.*, **331**, 137.
Noyes, R. W., Hartmann, L., Baliunas, S. L., Duncan, D. K., and Vaughan, A. H. 1984, *Ap. J.*, **279**, 763.
Noyes, R. W., Weiss, N. O., and Vaughan, A. H. 1984, *Ap. J.*, **287**, 769.
Scargle, J. D. 1982, *Ap. J.*, **263**, 835.
Skumanich, A., Lean, J. L., White, O. R., and Livingston, W. C. 1984, *Ap. J.*, **282**, 776.
Vaughan, A. H., Baliunas, S. L., Middelkoop, F., Hartmann, L., Mihalas, D., Noyes, R. W., and Preston, G. W. 1981, *Ap. J.*, **250**, 276.
Waldmeier, M. 1955, *Ergebnisse und Probleme der Sonnenforschung* (2d ed., Leipzig: Geest u. Portig).
White, O. R., and Livingston, W. C. 1978, *Ap. J.*, **226**, 679.
———. 1981, *Ap. J.*, **249**, 798.
Wilson, O. C. 1978, *Ap. J.*, **226**, 379.

SALLIE L. BALIUNAS: Center for Astrophysics, Mailstop 15, 60 Garden Street, Cambridge, MA 02138

RONALD L. GILLILAND: High Altitude Observatory, P.O. Box 3000, Boulder, CO 80307